J Mater Sci: Mater Electron (2015) 26:9630–9639
DOI 10.1007/s10854-015-3628-5

Micromorphology characterization of copper thin films by AFM and fractal analysis

Ali Arman[1] · Ştefan Ţălu[2] · Carlos Luna[3] · Azin Ahmadpourian[4] · Mosayeb Naseri[4] · Mehrdad Molamohammadi[1]

Received: 12 July 2015 / Accepted: 10 August 2015 / Published online: 18 August 2015
© Springer Science+Business Media New York 2015

Abstract In this study, Cu thin films with layer thicknesses of 5, 25, and 50 nm were prepared by DC magnetron-sputtering method and their three dimensional (3-D) surface topography were investigated. Concretely, the 3-D surface roughness of samples was studied by atomic force microscopy (AFM), fractal analysis of the 3-D AFM-images and power spectral density (PSD) function. Also the content of thin films was characterized by X-ray diffraction (XRD). The thin films were prepared onto glass and p-type silicon (100) substrates by DC magnetron-sputtering method and were studied over square areas of 4.4 μm × 4.4 μm using AFM and fractal analysis. The 3-D surface morphology revealed the fractal geometry of Cu thin films at nanometer scale, which can be quantitatively estimated by the fractal dimension D_f that was determined by cube counting method, based on the linear interpolation type. The results from AFM data indicated the possible presence of superstructures on the growth process of Cu nanostructures that were in relatively good agreement with XRD data and PSD.

✉ Ali Arman
ali.arman173@gmail.com

[1] Young Researchers and Elite Club, Kermanshah Branch, Islamic Azad University, Kermanshah, Iran

[2] Department of AET, Discipline of Descriptive Geometry and Engineering Graphics, Faculty of Mechanical Engineering, Technical University of Cluj-Napoca, 103-105 B-dul Muncii St., 400641 Cluj-Napoca, Cluj, Romania

[3] Facultad de Ciencias Físico Matemáticas, Universidad Autónoma de Nuevo León, Av. Pedro de Alba s/n, 66455 San Nicolás de los Garza, Nuevo León, Mexico

[4] Departments of Physics, Kermanshah Branch, Islamic Azad University, Kermanshah, Iran

1 Introduction

The synthesis of thin multilayer metallic films and the investigation of their properties have currently attracted more attention because of their applications in biocompatible materials, electronics and micromechanical devices [1–3]. In this regards, it is well known that the properties of the thin films are usually substantially influenced by their microstructure and surface morphology [4, 5]. Thus, the investigation of the surface morphology of multilayer metals plays an important role not only in understanding the growing processes of thin films but also in determining the structure of thin films in order to obtain better favorable physical and chemical properties [6–9].

During the past decade, three primary microscopic methods: atomic force microscopy (AFM), transmission electron microscopy (TEM), and scanning tunneling microscopy (STM), have been extensively utilized in high-tech industries to find correlations between the 3-D surface morphology of thin films and the material properties [10]. Among these methods, AFM analysis is probably the best and most commonly used to characterize thin film systems [11]. On the other hand, DC magnetron-sputtering method has become more important to fabricate pure Cu thin films due to its many advantages, such as high growth rate, low temperature deposition and good reproducibility [12].

In modern manufacturing processes, measuring the 3-D surface topography is critical to ensure the quality of production [13]. It is known that engineering surfaces are often random, isotropic or anisotropic, and either Gaussian or non-Gaussian [14, 15]. Different studies about the characterization of 3-D surface morphology of thin films have been reported in the literature [16–20], and in several of them, the 3-D topography of thin films obtained from AFM data have been characterized in terms of fractal [20–23]

and multifractal [24–28] geometry. It is known that the fractal/multifractal 3-D surface geometries are characterized by scaling independence and possess only statistical self-similarity, which takes place only in the restricted range of the spatial scales [21–23].

On the other hand, although Root Mean Square (RMS) roughness parameter provides more data about the 3-D surface morphology, it doesn't make any difference between peaks and valleys [20]. Therefore, power spectral density (PSD) function, which presents more useful 3-D surface morphology information [29, 30], was used in this study for better description of optimal multilayer coating.

In this work, Cu thin films with a face-centered cubic (fcc) structure have been prepared by the DC magnetron-sputtering method, finding that their physical properties are dependent on the substrate's nature and the layer deposition conditions, in agreement with previous investigations [31, 32]. AFM and fractal analysis were used to study the 3-D surface topography of Cu thin films.

2 Materials and methods

2.1 Experimental details

Three Cu thin films with 5, 25 and 50 nm in thickness (named samples #1, #2 and #3 respectively) were prepared onto glass and p-type silicon (100) substrates by DC magnetron-sputtering method. The film thickness ranged from 5 to 50 nm was controlled by a carefully calibrated quartz microbalance. The reactor consisted of two electrodes with different area size. The smaller electrode was a Cu plate with 0.05 m diameter as a powered electrode and the other electrode was grounded substrates. The distance between powered electrode and the substrate was maintained at 5 cm. The chamber was evacuated up to a pressure of 10^{-3} Pa by rotary and defusing pumps to the deposition. The identification, the parameters of synthesis and the final thickness of the prepared samples are given in Table 1.

2.2 Characterization of the Cu thin films

Characterization of film topography by AFM was conducted in non contact mode using a Nanoscope Multimode atomic force microscope (Digital Instruments, Santa Barbara, CA), using scan rates of 10–20 µm/s to obtain 256 × 256 pixel images. The experiments were carried out at room temperature (24 ± 1 °C) using cantilevers with the nominal properties for force-distance curve measurements. All images were obtained over square areas of 4.4 µm × 4.4 µm. The average particle size, Root Mean Square (RMS) roughness, power spectral density (PSD) and fractal dimension were obtained from AFM data [33].

The structure and lattice strain of the Cu thin film was investigated by XRD that suggested the formation of superlattices on these films. The average crystal size of Cu nanoparticles was compared by Williamson–Hall formula [34].

2.3 Characterization of the Cu thin films by power spectral density (PSD) function

The power spectral density function of the bidirectional reflectance distribution function (BRDF) has been delivered on base of the AFM surface profile data. In this work, the PSD function was determined by Eq. (1) [35]:

$$S_2(f_x, f_y) = \frac{1}{L^2}\left[\sum_{m=1}^{N}\sum_{n=1}^{N} Z_{mn} e^{-e\pi i \Delta L (f_x m + f_y n)} (\Delta L)^2\right]^2 \quad (1)$$

where S_2 denotes the two-dimensional PSD, L is the scanned surface area, N is the number of data points per line and row, Z_{mn} is the profile height at position (m, n), f_x, f_y are the spatial frequency in the x- and y-directions and $\Delta L = L/N$ is the sampling distance.

2.4 Fractal analysis of the Cu thin film 3-D surface

The fractal dimension D_f, as a quantitative parameter to globally estimate the 3-D fractal surface complexity, is a fractional value within the range $2 \leq D_f \leq 3$ [20, 21]. In literature, there are different computing methods to estimate the fractal dimension [15, 20–23]. In this study, the fractal analysis was applied to the original AFM files using the cube counting method (derived directly from a definition of box-counting fractal dimension) with a linear interpolation type [36]. A higher fractal dimension of 3-D surface structure indicates higher values of D_f [21–23].

Table 1 Details of prepared samples

ID	Target	DC magnetron sputtering parameters			Thickness (nm)
		Basic pressure (N/m^2)	Work pressure (N/m^2)	Power (W)	
#1	Cu	3×10^{-3}	2.9	20	5
#2	Cu	3×10^{-3}	2.9	20	25
#3	Cu	3×10^{-3}	2.9	20	50

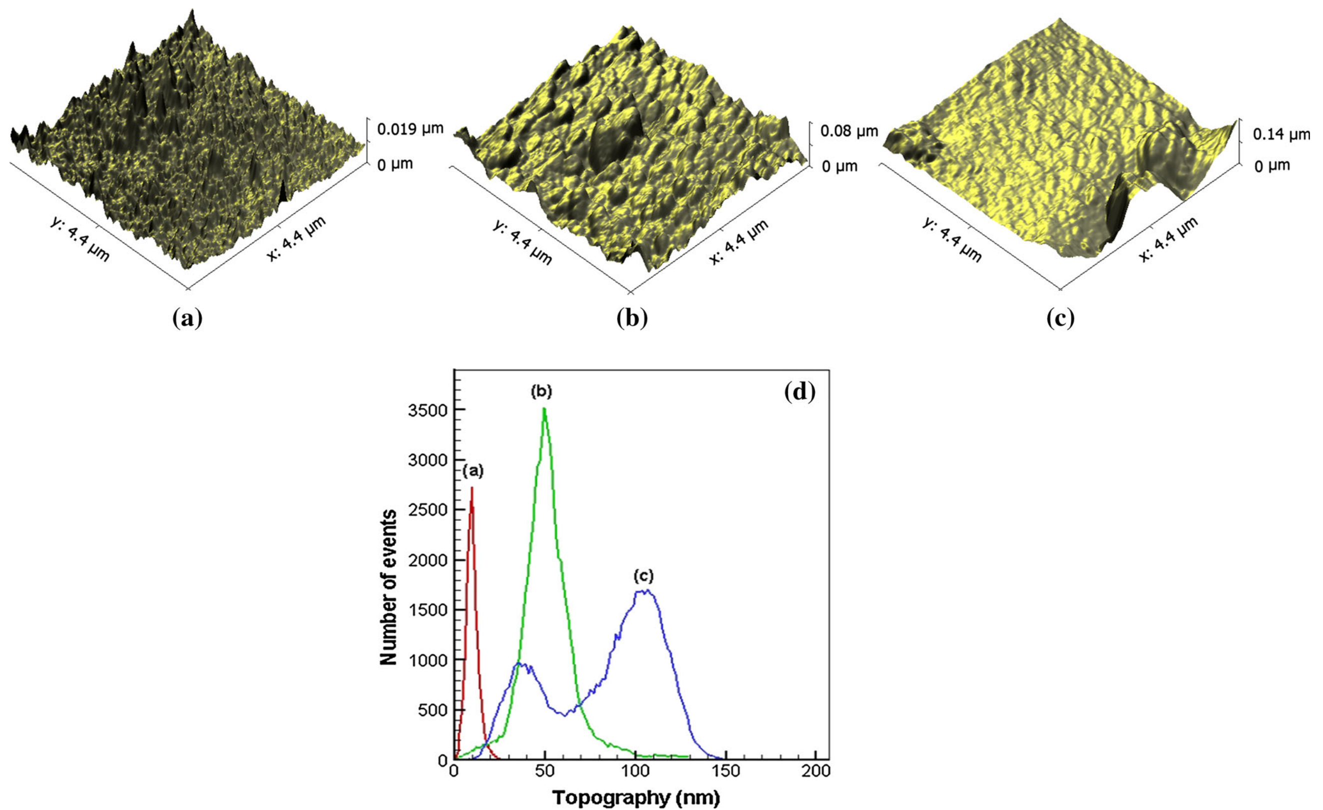

Fig. 1 Representative AFM images of samples **a** #1, **b** #2 and **c** #3 and their corresponding topography (**d**)

Table 2 The basic properties of the height values distribution (including its variance, skewness and kurtosis) of the surface samples, for scanning square areas of 4.4 µm × 4.4 µm

The basic properties of the height values distribution of the surface samples	Sample #1 Values	Sample #2 Values	Sample #3 Values
Ra (Sa) (nm)	2.67	10.8	14.8
Rms (Sq) (nm)	3.53	15.5	26.8
Skew (Ssk) (–)	−0.356	0.826	2.6
Kurtosis (Sku) (–)	−0.923	0.948	8.89
Inclination θ (°)	1.1	2.7	0.3
Inclination φ (°)	85.6	83.4	−33.3

2.5 Structural analysis of the Cu thin film 3-D surface

For structural analysis, the inter-plane spacing was obtained using the Bragg law [37]:

$$d_{hkl} = \frac{\lambda}{2}\sin\theta \quad (2)$$

The lattice strain and crystallite size were determined using the Williamson–Hall equation [34, 37]:

$$B\text{Cos}\theta = \frac{.9\lambda}{D} + 4\varepsilon Sin\,\theta \quad (3)$$

where θ is the Bragg angle of the peak, B is the measured FWHM (in radians), λ is the X-ray diffraction wavelength, D is the effective crystallite size, and ε is the effective strain.

Dislocations are an imperfection in a crystal associated with misregistry in the crystalline lattice in one part of the crystal with respect to another part. In fact growth mechanism involving dislocation is a matter of importance. The

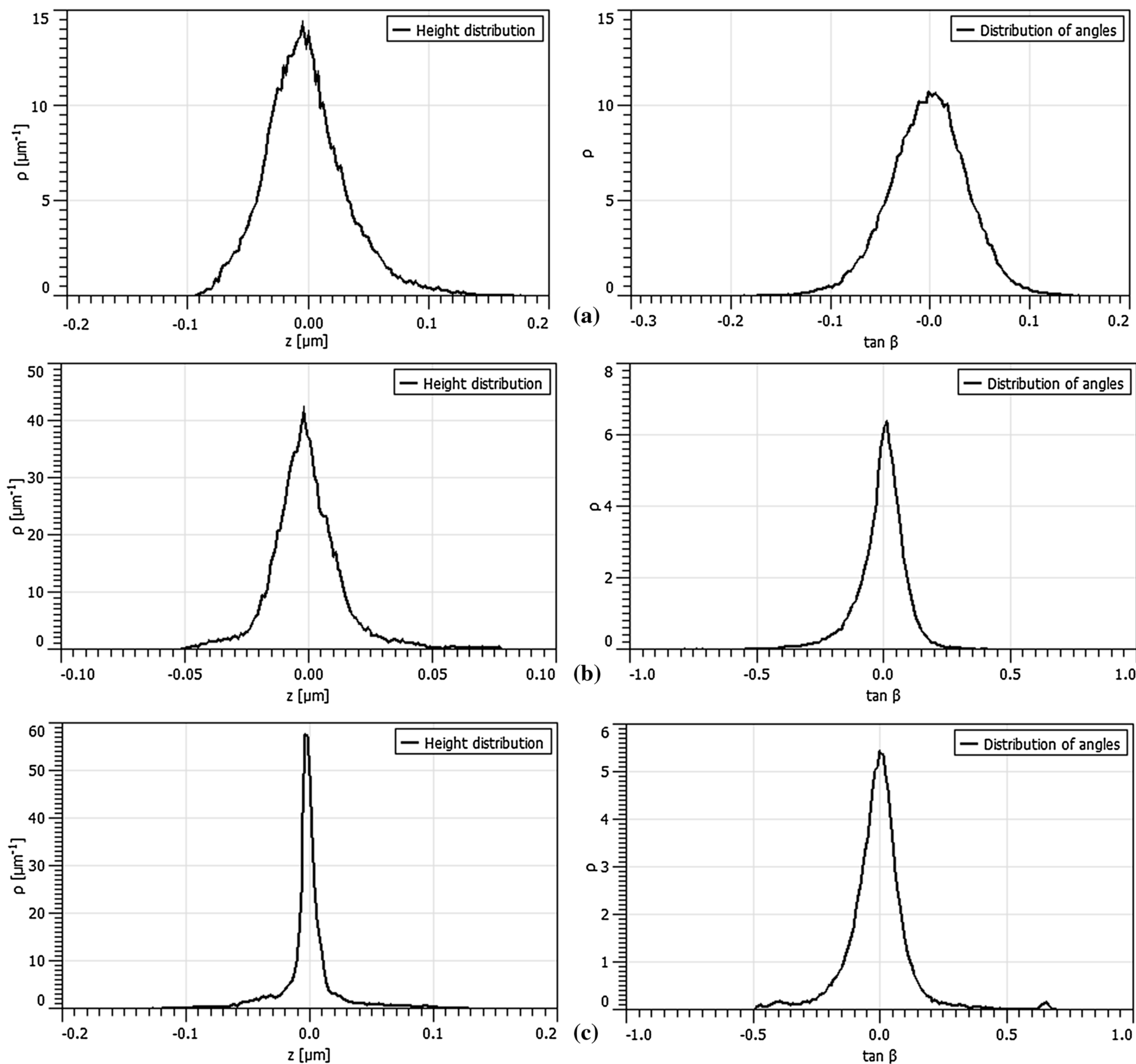

Fig. 2 The height and slope distribution functions for samples of Fig. 1 (where p is the corresponding quantity, height or slope; and abscissa is the tangent of the angle), computed as non-cumulative (i.e. densities) magnitudes: **a** sample #1, **b** sample #2, **c** sample #3. Scanning square areas of 4.4 μm × 4.4 μm

dislocation densities of thin films are given by the formula [38, 39]:

$$\delta = n/D^2 \quad (4)$$

where n is a factor that equals unity when the dislocation density is minimum and D is the grain size.

3 Results and discussion

The representative 3-D AFM images of samples #1, #2 and #3 for scanning areas of 4.4 μm × 4.4 μm, are shown in Fig. 1.

The maximum of abundance gives average of the particle size and its width gives the variance of radius the particle size [39]. It can be seen clearly from the Fig. 1d that as the layer thicknesses is increased, the surface morphology of the samples display two Gaussian contributions. This behavior is caused by the aggregation of the native grains into larger clusters and formation of new phase [40–42].

The basic properties of the height values distribution of the surface samples (including its variance, skewness and kurtosis), computed according the Ref. [36] is shown in Table 2, for scanning square areas of 4.4 μm × 4.4 μm.

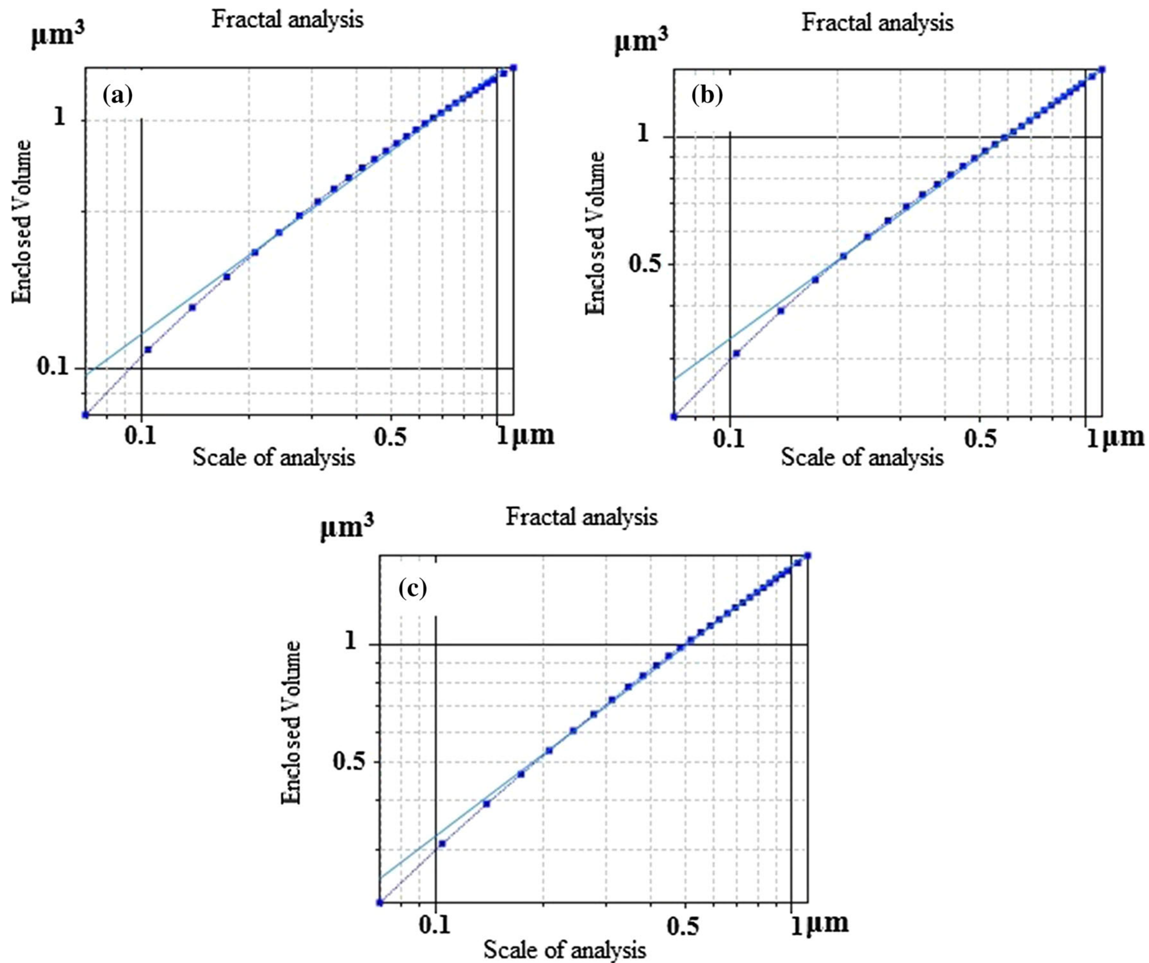

Fig. 3 The fractal dimension determined by morphological envelopes method for the three samples: **a** #1, **b** #2 and **c** #3

Table 3 The fractal dimensions (average ± SD) with coefficients of correlation (R^2) determined by the cube counting method, based on the linear interpolation type, for samples #1, #2 and #3

Parameters	#1	#2	#3
D_f	2.50 ± 0.01	2.39 ± 0.01	2.31 ± 0.01
R^2	0.992	0.992	0.992

It can be observed (Fig. 1; Table 2) that as the Rms (Sq) of samples increases as layers thickness increases. This behavior is due to the aggregation of particles and formation of new phase [41–43] The statistical properties of the individual points can be characterized with the height and slope distribution quantities, and are calculated according the Ref. [36].

In Fig. 2 are shown the height and slope distribution functions for the three samples of Fig. 1 (where p is the corresponding quantity, height or slope; and abscissa is the tangent of the angle), computed as non-cumulative (i.e. densities) magnitudes. It is observed that a maximum value

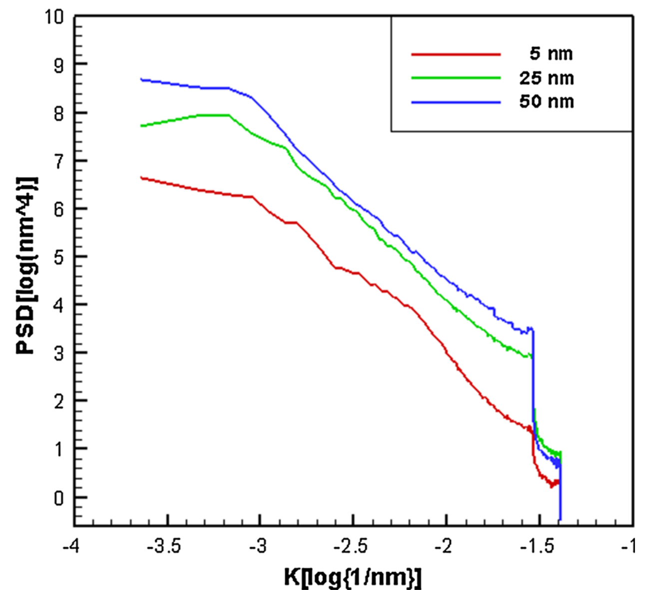

Fig. 4 Power spectra density P (k) versus frequency k for the Cu thin films

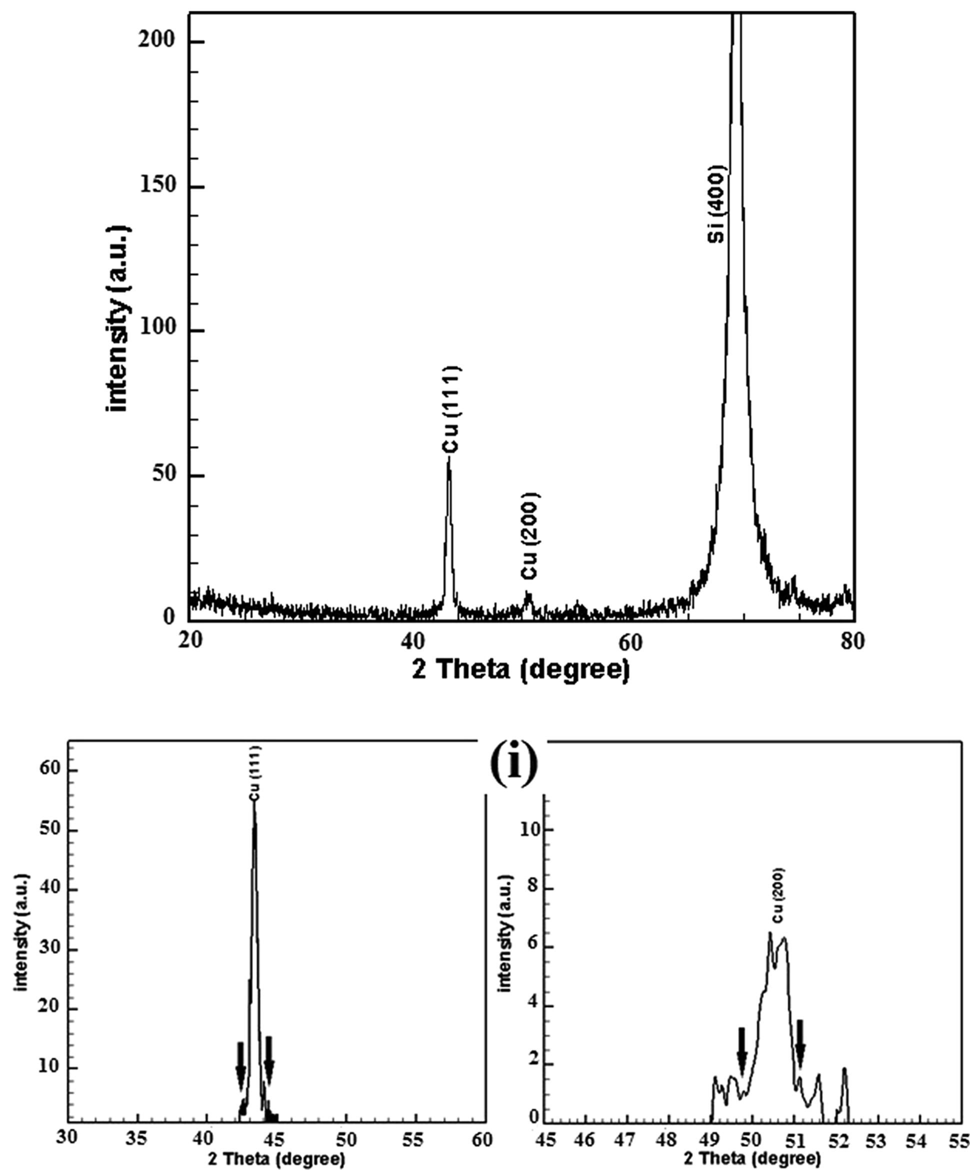

Fig. 5 X-ray Diffraction (XRD) of Cu thin film (sample #3)

Table 4 Structural information obtained from XRD patterns for the Cu thin films

Hkl	2θ (°)	d-spacing (d_{hkl}/nm)	Crystallite size (D/nm)	Strain ($\varepsilon \times 10^{-3}$)	Dislocation density ($\delta \times 10^{15}$)
111	43.49	0.119296	20	1.25	2.5

of corresponding quantity (ρ) for sample c; the curve increases for sample a, and decreases for sample c.

A summary of the fractal dimensions with coefficients of correlation (R^2) determined by the morphological envelopes method, based on the linear interpolation type, for samples #1, #2 and #3 are shown in Fig. 3. The coefficients of correlation (R^2) of all linear fits were equal to 0.992 representing a good linear correlation (Table 3).

The surface of sample #1 had the most irregular topography ($D_f = 2.50 \pm 0.01$) than those of all the other samples (#2 and #3).

Figure 4 shows the experimental PSD profiles of Cu thin films deposited with various thicknesses.

The rate of deposition and the film thickness have a major influence on the microroughness because, (as it can be seen clearly in Fig. 4) the morphology of the layer with 50 nm thickness exhibits higher PSD values than those of the other samples with lower PSD values, showing a slower variation, which it may be attributed to the formation of new smaller crystallites on the larger grains [20, 44, 45].

The PSD plots at lower spatial frequency region exhibited more than one local maximum that suggests the occurrence

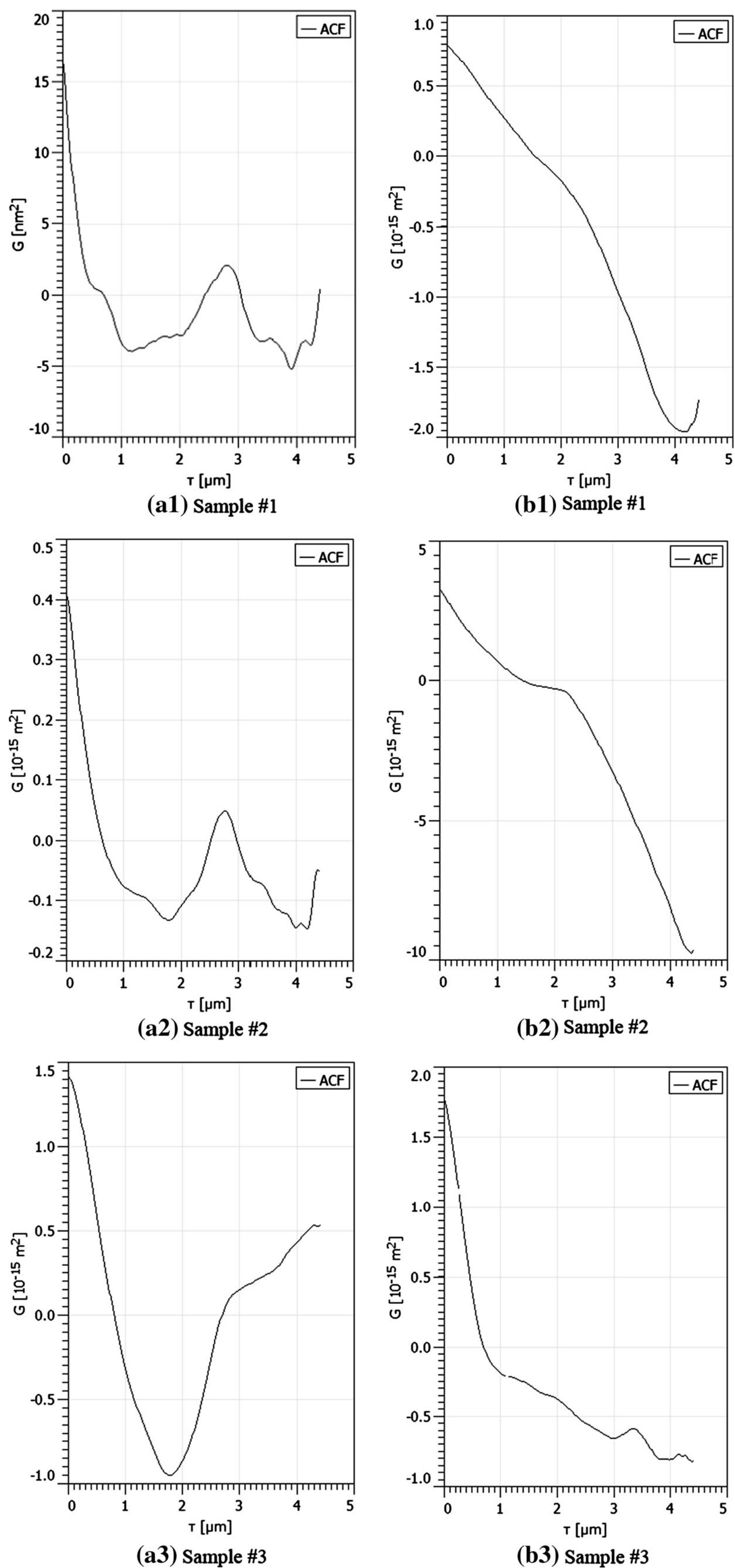

Fig. 6 The autocorrelation function (G), based on the linear interpolation type, for samples #1, #2 and #3: **a** *horizontal direction*, **b** *vertical direction*. Abscissa is the distance between these points τ. Scanning square areas of 4.4 μm × 4.4 μm

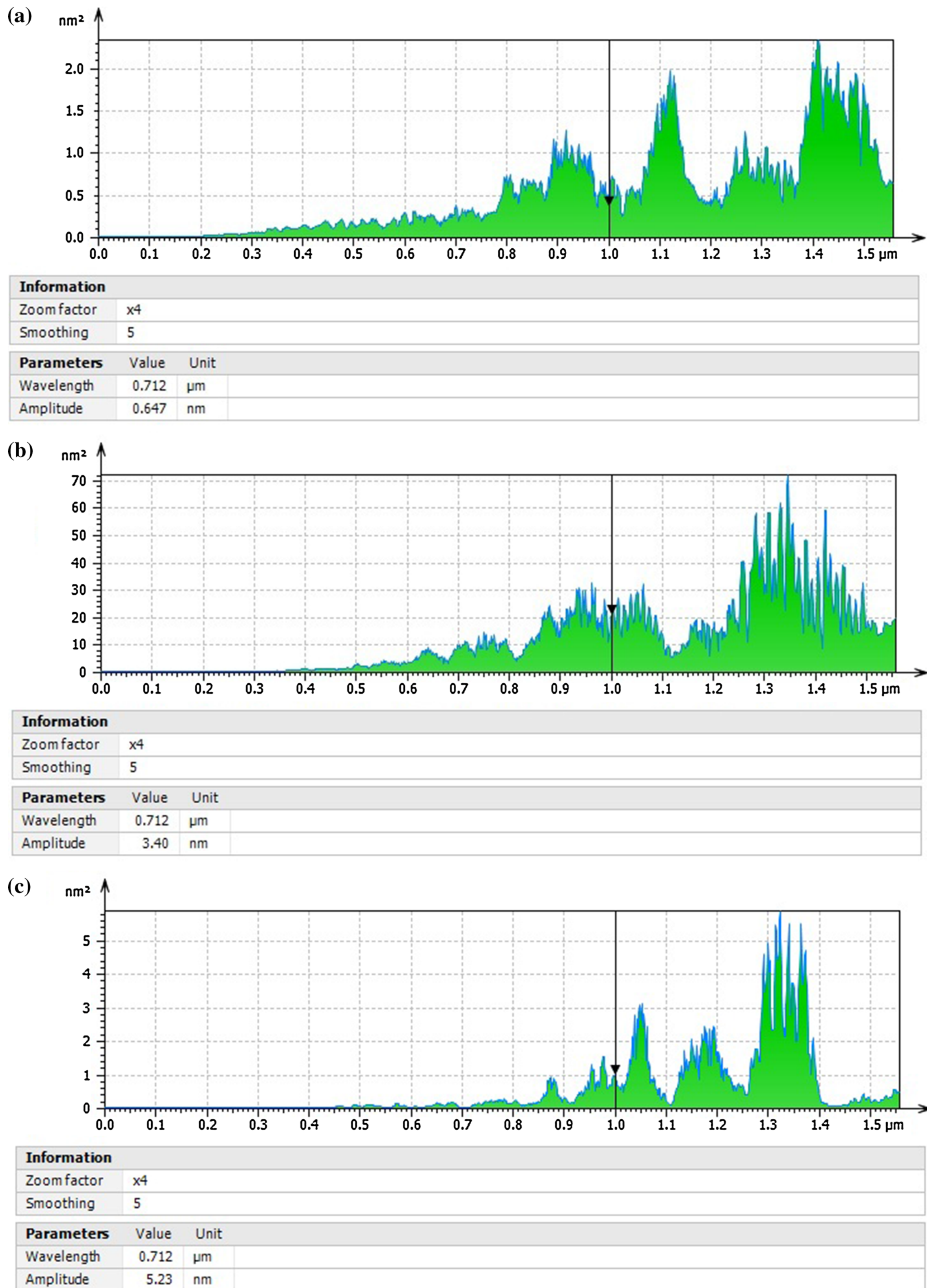

Fig. 7 The averaged power spectral density (surface) of: **a** sample #1, **b** sample #2, **c** sample #3, calculated for scanning square areas of 4.4 µm × 4.4 µm

of superstructures in the thin films [46]. Finally, the result of XRD provides an additional evidence of the existence and structural information of Cu nanocrystals in these films [40]. Figure 5 shows the XRD pattern of sample #3 that confirms the presence of fcc Cu nanocrystals with (1 1 1) and (2 0 0) orientations growth onto this film [40, 47].

Note that for the determination of the crystal size from the width of XRD peaks, the effects of the grains internal stress on the peaks width should be considered. In this regards, Williamson–Hall relation (that considers such effects) is a more useful tool to determine the crystal size than the Scherer's formula. In our results, it is found a non isotopic stress in the copper peaks which not only led to larger interplanar distances with respect to a prefect bulk crystal but also curvature of planes. Origin of this stress comes from finite-size effect of nanoparticles where the copper atoms are assembled in a nanoscopic volume.

Also, XRD results show that the deposited thin films have a preferred crystal orientation of [111] and [200], which suggests the superstructure formation in Fig. 5(i) [48, 49]. The structural information obtained from XRD patterns for Cu films is summarized in Table 4.

The mutual relationship of two points on the surface can be characterized using the second-order statistical quantities; these functions are namely the autocorrelation function (G) and the height–height correlation function (H) [36]. In Fig. 6 are shown the graphical representations of the autocorrelation function (ACF), based on the linear interpolation type, for samples #1, #2 and #3, in horizontal and vertical direction, for scanning areas of 4.4 μm × 4.4 μm.

The averaged power spectral density (surface) of samples #1, #2 and #3, was calculated for scanning square areas of 4.4 μm × 4.4 μm. (Figure 7).

4 Conclusions

In this study, the 3-D surface topography of Cu thin films with layer thicknesses of 5, 25, and 50 nm, prepared by DC magnetron-sputtering method, were analyzed. Concretely, the 3-D surface topography of samples was studied by AFM, XRD analysis, fractal analysis of the 3-D AFM-images and power spectral density (PSD) function.

The AFM images of Cu thin film surfaces of all samples highlight for every group a specific 3-D topography that can be characterized by the fractal dimensions. All these parameters can be included in algorithmic models to characterize local topography of the 3-D sample surfaces. PSD results indicate the presence of superstructure and a uniform growth mechanism in the films that are in relatively good agreement with the AFM images and the XRD data. This study confirms the results obtained by Gelali et al. [16] and Karimzadeh et al. [20].

Compliance with ethical standards

Conflict of interest The authors claim to have no financial interest, either directly or indirectly, in the products or information listed in the article.

Appendix

The basic properties of the height values distribution, including its variance, skewness and kurtosis, computed according the Ref. [36], were defined as follows:

- RMS value of the height irregularities: this quantity is computed from data variance.
- Ra value of the height irregularities: this quantity is similar to RMS value with the only difference that in exponent (power) within the data variance sum. As for the RMS this exponent is $q = 2$, the Ra value is computed with exponent $q = 1$ and absolute values of the data (zero mean).
- Height distribution skewness: computed from 3rd central moment of data values.
- Height distribution kurtosis: computed from 4th central moment of data values.
- Mean inclination of facets in area: computed by averaging normalized facet direction vectors.
- Variation, which is calculated as the integral of the absolute value of the local gradient.

References

1. S. Singh, B. Saibal, S.K. Ghosh, Appl. Surf. Sci. **255**(11), 5910–5916 (2009)
2. V. Weihnacht, W. Bruckner, Thin Solid Films **418**(2), 136–144 (2002)
3. T. Ghodselahi, A. Arman, J. Mater. Sci. Mater. Electron. **26**(6), 4193–4197 (2015)
4. A. Arman, T. Ghodselahi, M. Molamohammadi et al., Prot. Met. Phys. Chem. Surf. **51**(4), 575–578 (2015)
5. M. Molamohammadi, A. Arman, A. Achour et al., J. Mater. Sci. Mater. Electron. **26**(8), 5964–5969 (2015)
6. R. Gavrila, A. Dinescu, D. Mardare, Rom. J. Inf. Sci. Technol. **10**(3), 291–300 (2007)
7. J.H. Han, W.S. Yang, J.B. Yoo, C.Y. Park, J. Appl. Phys. **88**(12), 7363–7365 (2000)
8. Y.C. Choi, Y.M. Shin, Y.H. Lee, B.S. Lee, G.S. Park, W.B. Choi, N.S. Lee, J.M. Kim, Appl. Phys. Lett. **76**(17), 2367–2369 (2000)
9. M. Molamohammadi, C. Luna, A. Arman et al., J. Mater. Sci. Mater. Electron. **26**(9), 6814–6818 (2015)
10. J.M. Elson, J.M. Bennett, Appl. Opt. **34**(1), 201–208 (1995)
11. M. Bramowicz, S. Kulesza, K. Rychlik, Tech. Sci. Univ. Warm. Mazury Olszt. **15**, 307–318 (2012)
12. J.H. Boo, M.J. Jung, H.K. Park, K.H. Nam, J.G. Han, Surf. Coat. Technol. **188–189**, 721–727 (2004)

13. Ş. Ţălu, PhD. Researches concerning the cold rolling process of external cylindrical threads. Technical University of Cluj-Napoca, Cluj-Napoca, Romania (1998)
14. B. Bhushan, Analysis of surface roughness, in *Principles and Applications of Tribology*, 2nd edn., ed. by B. Bhushan (Wiley, New York, 2013), pp. 91–92
15. M. Bramowicz, S. Kulesza, T. Lipiński, P. Szabracki, P. Piątkowski, Solid State Phenom. **203–204**, 86–89 (2013)
16. A. Gelali, A. Ahmadpourian, S. Valedbagi, B. Safibonab, B. Astinchap, E. Karimzadeh, J. Basic Appl. Sci. Res. **3**(6), 846–849 (2013)
17. K.Y. Chan, B.S. Teo, Microelectron. J. **37**(10), 1064–1071 (2006)
18. K. Venkata Subba Reddy, A. Sivasankar Reddy, P. Sreedhara Reddy, S. Uthanna, J. Mater. Sci. Mater. Electron. **18**(10), 1003–1008 (2007)
19. K. Mech, R. Kowalik, P. Zabinski, Arch. Metall. Mater. **56**(4), 903–908 (2011)
20. E. Karimzadeh, A. Gelali, B. Astinchap, A. Ahmadpourian, B. Safibonab, A. Boochani, Eur. J. Sci. Res. **111**(4), 491–499 (2013)
21. S. Kulesza, M. Bramowicz, Appl. Surf. Sci. **293**, 196–201 (2014)
22. Ş. Ţălu, A.J. Ghazai, S. Stach, A. Hassan, Z. Hassan, M. Ţălu, J. Mater. Sci. Mater. Electron. **25**(1), 466–477 (2014)
23. D. Dallaeva, Ş. Ţălu, S. Stach, P. Škarvada, P. Tománek, L. Grmela, Appl. Surf. Sci. **312**, 81–86 (2014)
24. Q.J. Lin, S.M. Yang, C.Y. Wang, J.J. Ding, Z.D. Jiang, Surf. Interface Anal. **45**(8), 1223–1227 (2013)
25. Ş. Ţălu, S. Stach, A. Mahajan, D. Pathak, T. Wagner, A. Kumar, R.K. Bedi, Surf. Interface Anal. **46**(6), 393–398 (2014)
26. Ş. Ţălu, Z. Marković, S. Stach, B.T. Marković, M. Ţălu, Appl. Surf. Sci. **289**, 97–106 (2014)
27. Ş. Ţălu, S. Stach, A. Mahajan, D. Pathak, T. Wagner, A. Kumar, R.K. Bedi, M. Ţălu, Electron. Mater. Lett. **10**(4), 719–730 (2014)
28. Ş. Ţălu, S. Stach, A. Méndez, G. Trejo, M. Ţălu, J. Electrochem. Soc. **161**, D44–D47 (2014). doi:10.1149/2.039401JES
29. G. Binnig, C.F. Quate, C. Gerber, Phys. Rev. Lett. **56**(9), 930–933 (1986)
30. A. Arneodo, N. Decoster, S.G. Roux, Eur. Phys. J. B **15**, 567–600 (2000)
31. S.M. Cherif, A. Layadi, J. Ben Youssef, C. Nacereddine, Y. Roussigne, Phys. B Condens. Matter **387**(1–2), 281–286 (2007)
32. H.C. Barshilia, K.S. Rajam, Surf. Coat. Technol. **155**(2), 195–202 (2002)
33. I. Horcas, R. Fernandez, J.M. Gomez-Rodriguez, J. Colchero, J. Gomez-Herrero, A.M. Baro, Rev. Sci. Instrum. **78**(1), 013705 (2007)
34. A. Khorsand Zak, W.H.A. Majid, M.E. Abrishami, R. Yousefi, Solid State Sci. **13**(1), 251–256 (2011)
35. J. Ferre-Borrull, A. Duparre, E. Quesnel, Appl. Opt. **40**(13), 2190–2199 (2001)
36. Gwyddion 2.37 software (Copyright© 2004–2007, 2009–2014 Petr Klapetek, David Nečas, Christopher Anderson). http://gwyddion.net. Accessed 27 May 2015
37. H.L. Chen, Y.M. Lu, W.S. Hwang, Mater. Trans. **46**(4), 872–879 (2005)
38. D.P. Padiyan, A. Marikani, K.R. Murali, Mater. Chem. Phys. **78**(1), 51–58 (2002)
39. K. Sarmah, R. Sarma, H.L. Das, Chalcogenide Lett. **5**(8), 153–163 (2008)
40. T. Ghodselahi, M.A. Vesaghi, A. Gelali et al., Appl. Surf. Sci. **258**(2), 727–731 (2011)
41. D. Raoufi, Phys. B **405**(1), 451–455 (2010)
42. A. Gelali, A. Ahmadpourian, R. Bavadi, M.R. Hantehzadeh, A. Ahmadpourian, J. Fusion Energy **31**(6), 586–590 (2012)
43. V. Chawla, R. Jayaganthan, R. Chandra, Mater. Charact. **59**(8), 1015–1020 (2008)
44. S. Lalitha, R. Sathyamoorthy, S. Senthilarasu, A. Subbarayan, K. Natarajan, Sol. Energy Mater. Sol. Cells **82**(1–2), 187–199 (2004)
45. M. Öztas, M. Bedir, Thin Solid Films **516**(8), 1703–1709 (2008)
46. N.K. Sahoo, S. Thakur, R.B. Tokas, Thin Solid Films **503**(1–2), 85–95 (2006)
47. J. Ramyadevi, K. Jeyasubramanian, A. Marikani, G. Rajakumar, A.A. Rahuman, Mater. Lett. **71**, 114–116 (2012)
48. S.K. Ghosh, P.K. Limaye, B.P. Swain, N.L. Soni, R.G. Agrawal, R.O. Dusane, A.K. Grover, Surf. Coat. Technol. **201**(8), 4609–4618 (2007)
49. H. Zhang, W. Wang, Microsyst. Technol. **9**(6–7), 436–440 (2003)